The SARS-CoV-2 main protease Mpro causes microvascular brain pathology by cleaving NEMO in brain endothelial cells

Josephine Lampe
University of Lübeck
Jan Wenzel
University of Lübeck
Helge Müller-Fielitz
University of Lübeck https://orcid.org/0000-0003-2815-4426
Kristin Müller
University of Lübeck
Raphael Schuster
University of Lübeck
Linlin Zhang
University of Lübeck
Marietta Zille
University of Lübeck https://orcid.org/0000-0002-0609-8956
Markus Krohn
University of Lübeck
Ümit Özorhan
University of Lübeck https://orcid.org/0000-0002-7661-2818
Yun Jiang
University of Luebeck https://orcid.org/0000-0002-2886-7373
Vanessa Neve
University of Lübeck
Anke Fähnrich
University of Lübeck
Fabian Ott
University of Lübeck
Sonja Binder
University of Lübeck
Hauke Busch
University of Lübeck
Ludovic Collin

Roche Innovation Center Basel
Roberto Villasenor
Roche Innovation Center Basel
Olaf Jöhren
University of Lübeck
Hermann Altmeppen
University Medical Center Hamburg https://orcid.org/0000-0001-9439-6533
Manolis Pasparakis
University of Cologne https://orcid.org/0000-0002-9870-0966
Ruben Nogueiras
Department of Physiology, CIMUS, University of Santiago de Compostela-Instituto de Investigación Sanitaria, Santiago de Compostela, 15782, Spain https://orcid.org/0000-0002-9976-9930
Vincent Prevot
Inserm https://orcid.org/0000-0001-7185-3615
Rolf Hilgenfeld
University of Lübeck
Markus Glatzel
University Medical Center Hamburg-Eppendorf https://orcid.org/0000-0002-7720-8817
Markus Schwaninger (**markus.schwaninger@uni-luebeck.de**)
University of Lübeck https://orcid.org/0000-0002-4510-9718

Article

Keywords: SARS-CoV-2, microvascular brain pathology, NEMO

Posted Date: October 14th, 2020

DOI: https://doi.org/10.21203/rs.3.rs-86988/v1

Version of Record: A version of this preprint was published at Nature Neuroscience on October 21st, 2021. See the published version at https://doi.org/10.1038/s41593-021-00926-1.

Abstract

Several lines of evidence suggest that neurological symptoms in COVID-19 patients are partially due to damage to small vessels. However, the potential mechanisms are unclear. Here, we show that brain endothelial cells express SARS-CoV-2 receptors. The main protease of SARS-CoV-2 (M^{pro}) cleaves NEMO, the essential modulator of NF-κB signaling. By ablating NEMO, M^{pro} induces the death of human brain endothelial cells and a microvascular pathology in mice that is similar to what we find in the brain of COVID-19 patients. Importantly, the inhibition of receptor-interacting protein kinase (RIPK) 3, a mediator of regulated cell death, blocks the vessel rarefaction and disruption of the blood-brain barrier due to NEMO ablation. Our data suggest RIPK as a therapeutic target to treat the neuropathology of COVID-19.

Authors Josephine Lampe, Jan Wenzel, and Helge Müller-Fielitz contributed equally to this work.

Introduction

Starting in December 2019, the newly discovered coronavirus SARS-CoV-2 has caused the coronavirus disease 2019 (COVID-19)[1-3]. Within a few months, COVID-19 has developed into a pandemic with millions of people infected worldwide and a high death load[4]. Symptoms typically originate from the respiratory tract. However, many patients also suffer from the involvement of other organ systems that is not secondary to respiratory failure or the severe systemic inflammation due to pneumonia. A considerable proportion of patients, up to 84% of those with severe COVID-19, show neurological signs and symptoms including anosmia, epileptic seizures, strokes, loss of consciousness, and confusion[5-9]. Typically, COVID-19 can present with the clinical picture of encephalopathy[8]. The detection of SARS-CoV-2 viral genomes in the brain and cerebrospinal fluid (CSF) of some patients has supported the notion that SARS-CoV-2 gains access to the brain[10-12]. Viral RNA has been found in blood and virus-like particles or viral proteins in brain endothelial cells[10,13,14], suggesting that SARS-CoV-2 reaches the brain by a hematogenous route. In line with a vascular infection, endothelial cells in other organs have been identified as targets of SARS-CoV-2 infection[15,16]. In COVID-19 patients, magnetic resonance imaging detected lesions that are compatible with a microvascular pathology[17-21]. Autopsy studies have confirmed this interpretation[17,22-24]. However, the mechanisms that lead to small vessel disease in COVID-19 are still unclear.

The pathogenicity of viruses depends on their ability to manipulate host cells. There is evidence that SARS-CoV-2 proteins interact with the cellular machinery in various ways, including the cleavage of host proteins by viral proteases[25,26]. The SARS-CoV-2 genome encodes two viral proteases that are responsible for processing the viral polyproteins into the individual components of the replication and transcription complexes. We found that one of them, the main protease of SARS-CoV-2 M^{pro} (also called Nsp5 or $3CL^{pro}$)[27], cleaves the host protein NF-kappa-B essential modulator (NEMO). NEMO is involved in signaling cascades that regulate the transcription of numerous genes, including the anti-viral type I interferons and other immune genes[28]. Beyond gene regulation, NEMO modulates cell survival and prevents apoptosis and necroptosis[29]. The ablation of NEMO in brain endothelial cells induced

microvascular pathology in mice that was reminiscent of what we observed in brains of COVID-19 patients. Of note, the widespread death of endothelial cells, rarefaction of capillaries, disruption of the blood-brain barrier (BBB), and neuroinflammation due to NEMO ablation were prevented by deleting receptor-interacting protein kinase 3 (*Ripk3*), a protein kinase that is essential for regulated cell death. These data suggest RIPK3 inhibitors as a therapeutic option to interfere with the neurological consequences of COVID-19.

Results

Brain endothelial cells express SARS-CoV-2 receptors

To approach the question of how SARS-CoV-2 can infect brain endothelial cells, we determined the expression of membrane receptors and enzymes that are known to facilitate the entry of SARS-CoV-2 in host cells, namely angiotensin-converting enzyme 2 (ACE2), neuropilin-1 (Nrp1), basigin (Bsg), CD209A, Cd209b, Cd209c, Cd209d, and Tmprss2[9,14,30–32]. When analyzing isolated mouse brain cells by single-cell RNA sequencing (sc-RNA-seq), we identified 20 cell clusters, including two endothelial clusters (Extended data Fig. 1a,b). Some cells in the endothelial cell cluster 2 expressed *Ace2*, albeit at a lower level than pericytes (Fig. 1a). Imaging confirmed that ACE2 was expressed in cerebral microvessels but co-staining of endothelial and pericytic markers and high-resolution microscopy demonstrated that ACE2 was mainly localized in pericytes (Fig. 1a). In contrast, we observed high levels of *Nrp1* and *Bsg* expression in endothelial cells by sc-RNA-seq and immunostaining (Fig. 1b,c), but no *Cd209a-d* or *Tmprss2* (Extended data Fig. 1c-e). In summary, NRP1, BSG, and possibly ACE2 are potential receptors mediating the infection of brain endothelial cells by SARS-CoV-2.

M^{pro} cleaves NEMO

SARS-CoV-2-infected cells produce specific viral proteins. A strong immune response in COVID-19 patients implies that the viral main protease M^{pro} is expressed at a high level[33]. With respect to potential host substrates of M^{pro}, we speculated that it could be a successful strategy for SARS-CoV-2 to cleave NEMO as an essential component of the anti-viral immune response[34]. Indeed, purified M^{pro} cleaved recombinant human NEMO as well as human and mouse NEMO in extracts of brain endothelial or HEK293T cells in a dose- and time-dependent manner (Fig. 2a,b; Extended data Fig. 2, Extended data Fig. 3a,b). Importantly, M^{pro} cleaved NEMO also in intact brain endothelial cells (Fig. 2c). When co-expressed with NEMO-2A-GFP that self-processes to NEMO-2A and GFP, HA-tagged M^{pro} completely neutralized NEMO-2A in human hCMEC/D3 cells (Fig. 2c), although the GFP signal persisted (Extended data Fig. 3c), indicating that M^{pro} degraded NEMO.

In vitro, M^{pro} produced several NEMO fragments (Fig. 2a, Extended data Fig. 2). Tryptic digestion of M^{pro}-treated NEMO followed by mass spectrometry of the generated peptides showed that cleavage occurred

at Q83, Q205, Q231, Q304, and Q313 (Fig. 2d-e, Extended data Fig. 4). The cleavage sites that we have identified (Extended data Fig. 4k) resemble other known recognition sequences of M^{pro} (reference [27]). We verified the cleavage at Q231 by using synthetic peptides as substrates corresponding to both the human and mouse NEMO sequence (Fig. 2f, Extended data Fig. 5a-c). With the human NEMO sequence at Q231, the apparent catalytic efficiency (about 43 $s^{-1}M^{-1}$) was in the range that has been reported for the cleavage site between Nsp4 and Nsp5 (Extended data Fig. 5d)[35]. In keeping with the central role of Q in the recognition sequence, the mutation Q231A in the human NEMO sequence prevented cleavage by M^{pro} (Fig. 2f).

NEMO is an essential component of the canonical pathway leading to the activation of NF-κB by inflammatory factors such as interleukin (IL)-1β. Supporting the functional relevance of NEMO cleavage, M^{pro} blocked NF-κB activation. When expressed in human brain endothelial hCMEC/D3 cells, M^{pro} prevented the nuclear translocation of the NF-κB subunit p65, reflecting its activation in response to IL-1β (Fig. 3a). M^{pro} also abolished the stimulation of NF-κB-mediated gene transcription by IL-1β, which we investigated in hCMEC/D3 cells and mouse brain endothelial bEnd.3 cells using luciferase reporter gene assays (Fig. 3b,c). Thus, we obtained unequivocal evidence that M^{pro} cleaves and thereby inactivates NEMO.

M^{pro}-induced damage mimics microvascular pathology in COVID-19 patients

As NEMO is required for the integrity of some but not all cell types[29], the question arose whether the M^{pro}-mediated cleavage of NEMO compromises endothelial survival. To test whether M^{pro} induces endothelial cell death, we transfected hCMEC/D3 cells with a plasmid encoding for M^{pro}-HA and treated the cells with tumor necrosis factor (TNF) to model the elevated TNF serum concentrations in COVID-19 patients[36]. M^{pro}-expressing cells were more often positive for the cell death marker TUNEL, especially when exposed to TNF (Fig. 3d), demonstrating that M^{pro} promotes endothelial cell death.

To explore the function of M^{pro} *in vivo*, we employed the vector AAV-BR1 that selectively targets brain endothelial cells when injected intravenously[37]. After administering the control vector AAV-BR1-GFP, about 10% of cerebral capillaries expressed GFP (Fig. 3e,f). When mice had received AAV-BR1-M^{pro} two weeks before, we observed a decreased vascular density and an increased number of empty basement membrane tubes in their brains (Fig. 3g,h; Extended data Fig. 6). These so-called string vessels have been reported as a sign of microvascular pathology[38]. They appeared as thin structures with a typical diameter of 0.5–1 µm. Double staining of the vascular basement membrane marker collagen IV and the endothelial marker CD31 revealed that they did not contain endothelial cells.

Importantly, we also found string vessels in the brain of patients that had died with a SARS-CoV-2 infection (Fig. 3i). As in mice, string vessels appeared as thin basement membrane tubes. In the frontal

cortex of six patients with SARS-CoV-2 infection, the density of string vessels was higher than in six age- and sex-matched control patients (Fig. 3i, Extended data Table 1).

Capillaries are at risk from ablating NEMO

To confirm that the vascular pathology induced by M^{pro} is linked to NEMO ablation, we used a mouse model of inducible *Nemo* deletion in brain endothelial cells ($Nemo^{beKO}$)[39]. Similar to the M^{pro}-mediated cleavage of NEMO, its genetic ablation led to numerous string vessels in the brain (Fig. 4a,b; Extended data Fig. 7a). STED microscopy showed that string vessels are tube-like structures with a similar morphology in humans and $Nemo^{beKO}$ mice (Fig. 4b, Extended data Fig. 7a). They were deficient of endothelial cells. Our interpretation of string vessels as a sign of ongoing endothelial demise is based on the following observations. NEMO inactivation induced endothelial cell death as detected by staining for active caspase 3 or the TUNEL reaction (Fig. 4c,d). The death of endothelial cells typically occurred in vessel segments adjacent to string vessels (Fig. 4c,d). Most of them were observed in place of higher-order capillaries (Fig. 4e, Extended data Fig. 7b,c), suggesting that capillaries are particularly susceptible to NEMO deficiency. Consequently, small-diameter vessels were predominantly lost and mice developed patchy cerebral hypoxia (Fig. 4f,g). Finally, NEMO ablation led to a significant vessel rarefaction in the brain (Fig. 5a).

The loss of endothelial cells induced by NEMO deficiency also affected other cell types in the neurovascular unit. While the overall coverage of vessels by pericytes was slightly lowered (Fig. 4h), the number of microglia increased and they exhibited an activated morphology (Fig. 4i). The astrogliosis marker GFAP was strongly upregulated, indicating an inflammatory response (Fig. 4j).

RIPK3 mediates microvascular pathology induced by NEMO ablation

Microglia orchestrate the neuroinflammatory response in the brain, including the activation of astrocytes[40]. Therefore, we tested their role in the microvascular pathology induced by NEMO deficiency. However, ablating microglia by administering the CSF-1R antagonist PLX5622 did neither prevent the formation of string vessels nor the activation of astrocytes (Extended data Fig. 8).

To develop alternative therapeutic options, we considered previous reports that NEMO blocks apoptosis or necroptosis in epithelial cells[29]. In $Nemo^{beKO}$ mice, we inactivated the Fas-associated death domain protein (FADD), a component of apoptosis signaling, and RIPK3, a kinase central for both necroptosis and apoptosis (Extended data Fig. 9a). Unexpectedly, FADD deficiency did not ameliorate the consequences of *Nemo* deletion but significantly enhanced the damage induced by NEMO ablation (Extended data Fig. 9b-f). The deletion of only *Fadd* in brain endothelial cells led to the formation of string vessels and a disruption of the BBB as shown by the extravasation of IgG and albumin as well as brain edema

(Extended data Fig. 9b-d). Consequently, *Nemo*^{beKO}*Fadd*^{beKO} mice died within 9 days after tamoxifen injection inducing recombination and knockout (Extended data Fig. 9e).

In contrast, RIPK3 deficiency, which by itself did not affect the cerebral microvasculature, prevented the formation of string vessels and the rarefaction of cerebral vessels due to NEMO ablation (Fig. 5a). Probably as a response to the vessel rarefaction, NEMO deficiency stimulated endothelial proliferation indicating angiogenesis, which has been described in COVID-19 patients before[15]. Notably, *Ripk3* deletion abrogated endothelial proliferation (Fig. 5a). *Ripk3* deletion also normalized survival, brain weight, and body weight of mice with a NEMO deficiency in brain endothelial cells and reduced the extravasation of IgG and albumin into the parenchyma, showing that disruption of the BBB was mitigated (Fig. 5b,c; Extended data Fig. 9d,f). Consequentially, NEMO ablation did not activate microglia or astrocytes in the absence of RIPK3 (Fig. 5d).

To explore the mechanisms of BBB protection by RIPK3 deficiency, we quantified the levels of the tight junction protein occludin. NEMO deficiency led to interruptions and the disintegration of occludin^{+} tight junctions, which was prevented by RIPK3 deficiency (Fig. 5e). In addition to endothelial tight junctions, the BBB is characterized by a low rate of transcytosis in cerebral capillaries. The increased IgG extravasation in *Nemo*^{beKO} mice was associated with a lower number of IgG-filled vesicles in brain endothelial cells (Fig. 5f). While this may seem counterintuitive, we have observed a similar reduction of IgG-filled vesicles despite increased overall IgG extravasation in *Pdgfb*$^{ret/ret}$ mice, demonstrating that the detected population of IgG-filled vesicles limit IgG permeation across the BBB[41,42]. RIPK3 deficiency did not counteract the effect of NEMO ablation on IgG transcytosis (Fig. 5f). Therefore, we conclude that RIPK3 deficiency improves the BBB tightness of *Nemo*^{beKO} mice mainly by preventing endothelial cell death and rescuing tight junctions. Overall, these data suggest that inhibitors of RIPK3 signaling may protect against the microvascular pathology induced by M^{pro} and SARS-CoV-2 infection.

Discussion

In many COVID-19 patients, neurological symptoms occur during the acute disease and possibly also as a late consequence[43]. Here, we show microvascular pathology in the brain of COVID-19 patients and propose a mechanism by which SARS-CoV-2 infection compromises brain endothelial function, damages the BBB, and reduces CNS perfusion.

Our data demonstrate that M^{pro} of SARS-CoV-2 cleaves host cell NEMO with high efficiency. In infected cells, M^{pro} is located in the cytosol and nucleus, where NEMO is also present[44,45]. Cleavage by M^{pro} inactivated NEMO. This may benefit the virus by preventing the induction of anti-viral type I interferons that depend on NEMO[28]. Indeed, levels of type I interferons are low or absent in the peripheral blood of COVID-19 patients[46,47]. Cleaving NEMO is also a strategy used by other viruses[48–50]. However, the tropism of SARS-CoV-2 is likely to limit NEMO inactivation to specific cell types. Accordingly, some NF-κB-dependent cytokines, such as TNF and IL-6, are highly upregulated, indicating that the cells of origin have

escaped NEMO inactivation[47]. In contrast, several studies report evidence that SARS-CoV-2 infects endothelial cells[10,14,15,51]. In support, we find the SARS-CoV-2 receptors Nrp1, Bsg, and Ace2 expressed in brain endothelial cells. In addition to its central role in immunity, NEMO supports the survival of some but not all cell types [29]. While neurons, glia, and endothelial cells of peripheral vessels seem to resist NEMO deficiency or are even protected by it against inflammatory stimuli[52,53], the survival of other cells, including brain endothelial cells, is supported by NEMO. Our data suggest that, in COVID-19, brain endothelial cells are at disproportionate risk when being infected by SARS-CoV-2 because of their dependence on NEMO activity for survival.

Cleavage of NEMO by M^{pro} mimics the rare genetic disease *incontinentia pigmenti* that is caused by inactivating mutations in the *NEMO* (*IKBKG*) gene. In the latter condition, patients suffer from a mix of neurological symptoms, such as encephalopathy, stroke, and seizures that resemble neurological manifestations of COVID-19[54,55]. The absence of NEMO induced a loss of endothelial cells and microvascular pathology. Subsequently, patchy hypoxia developed in the brain and the BBB became leaky. In parenchymal cells, a prominent upregulation of GFAP indicated the activation of astrocytes, in line with the finding that GFAP concentrations are elevated in the blood of COVID-19 patients[56]. An increased BBB permeability and astrocyte activation may cause epileptic seizures in COVID-19 patients as in *incontinentia pigmenti*[54,55,57].

M^{pro}-mediated damage of brain endothelial cells suggests that inhibitors of M^{pro} (reference [27]) may prevent neurological complications of the SARS-CoV-2 infection. Another therapeutic approach may arise from the observation that deletion of *Ripk3* profoundly improved the microvascular pathology. RIPK1 and RIPK3 inhibitors are available and have already entered phases of clinical testing[58–60] suggesting therapeutic options for COVID-19 as well as for *incontinentia pigmenti*.

Declarations

Competing interests

L.C. and R.V. are under paid employment by Hoffman La Roche.

Author contributions

J.L., J.W., H.M.F., and M.S. designed the study. J.L., J.W., H.M.F., K.M., R.S., M.Z., M.K., Y.J., Ü.Ö., V.N., A.F., F.O., S.B., H.B., L.C., R.V., and O.J. performed experiments and analyzed the data. L.C., R.V., O.J., M.P., R.H., M.G., R.N., and V.P. provided tools, samples and conceptual support. J.L., J.W., H.M.F., R.N., V.P. and M.S. drafted the article. All authors revised the manuscript for important intellectual content.

Acknowledgements

We would like to thank Frauke Spiecker, Beate Lembrich, and Wiebke Brandt for expert technical help. PLX5266 was kindly provided by Plexxikon Inc. This work was supported by the European Research Council (ERC) Synergy Grant-2019-WATCH-810331 to V. P., R. N., and M. S., by grants of the Deutsche Forschungsgemeinschaft (DFG) SCHW 416/5 – 3, INST 392/135-1 to M. S., SFB1403 [project no. 414786233] to M.P., SFB877 to M.G., by the European Union´s Horizon 2020 research and innovation programme under the Marie Skłodowska-Curie grant agreement No. 813294 (ENTRAIN) to J.W. and M.S., and a Roche RiSE fellowship (2017–2018) to J.L.. Work in the Hilgenfeld laboratory was supported by the European Commission through its SCORE programme (grant agreement no. 101003627).

References

1. Huang, C., *et al.* Clinical features of patients infected with 2019 novel coronavirus in Wuhan, China. *Lancet* **395**, 497–506 (2020).
2. Wu, F., *et al.* A new coronavirus associated with human respiratory disease in China. *Nature* **579**, 265–269 (2020).
3. Zhu, N., *et al.* A Novel Coronavirus from Patients with Pneumonia in China, 2019. *N Engl J Med* **382**, 727–733 (2020).
4. WHO. 02.10.2020. https://www.who.int/docs/default-source/coronaviruse/20200630-covid-19-sitrep-162.pdf?sfvrsn=e00a5466_2.
5. Helms, J., *et al.* Neurologic Features in Severe SARS-CoV-2 Infection. *N Engl J Med* **382**, 2268–2270 (2020).
6. Chen, T., *et al.* Clinical characteristics of 113 deceased patients with coronavirus disease 2019: retrospective study. *BMJ* **368**, m1091 (2020).
7. Mao, L., *et al.* Neurologic Manifestations of Hospitalized Patients With Coronavirus Disease 2019 in Wuhan, China. *JAMA Neurol* **77**, 683–690 (2020).
8. Paterson, R.W., *et al.* The emerging spectrum of COVID-19 neurology: clinical, radiological and laboratory findings. *Brain* (2020).
9. Iadecola, C., Anrather, J. & Kamel, H. Effects of COVID-19 on the Nervous System. *Cell* **183**, 16–27.e11 (2020).
10. Paniz-Mondolfi, A., *et al.* Central nervous system involvement by severe acute respiratory syndrome coronavirus-2 (SARS-CoV-2). *J Med Virol* **92**, 699–702 (2020).
11. Zhou, L., Zhang, M., Wang, J. & Gao, J. Sars-Cov-2: Underestimated damage to nervous system. *Travel Med Infect Dis* **36**, 101642 (2020).
12. Moriguchi, T., *et al.* A first case of meningitis/encephalitis associated with SARS-Coronavirus-2. *Int J Infect Dis* **94**, 55–58 (2020).

13. Andersson, M., *et al.* SARS-CoV-2 RNA detected in blood samples from patients with COVID-19 is not associated with infectious virus. *medRxiv*, 2020.2005.2021.20105486 (2020).
14. Cantuti-Castelvetri, L., *et al.* Neuropilin-1 facilitates SARS-CoV-2 cell entry and provides a possible pathway into the central nervous system. *bioRxiv*, 2020.2006.2007.137802 (2020).
15. Ackermann, M., *et al.* Pulmonary Vascular Endothelialitis, Thrombosis, and Angiogenesis in Covid-19. *N Engl J Med* **383**, 120–128 (2020).
16. Varga, Z., *et al.* Endothelial cell infection and endotheliitis in COVID-19. *The Lancet* **395**, 1417–1418 (2020).
17. Conklin, J., *et al.* Cerebral Microvascular Injury in Severe COVID-19. *medRxiv* (2020).
18. Kremer, S., *et al.* Brain MRI Findings in Severe COVID-19: A Retrospective Observational Study. *Radiology*, 202222 (2020).
19. Nicholson, P., Alshafai, L. & Krings, T. Neuroimaging Findings in Patients with COVID-19. *AJNR. American journal of neuroradiology* **41**, 1380–1383 (2020).
20. Radmanesh, A., *et al.* COVID-19-associated Diffuse Leukoencephalopathy and Microhemorrhages. *Radiology* **297**, E223-E227 (2020).
21. Sachs, J.R., *et al.* COVID-19-associated Leukoencephalopathy. *Radiology* **296**, E184-E185 (2020).
22. Jaunmuktane, Z., *et al.* Microvascular injury and hypoxic damage: emerging neuropathological signatures in COVID-19. *Acta Neuropathol* **140**, 397–400 (2020).
23. Reichard, R.R., *et al.* Neuropathology of COVID-19: a spectrum of vascular and acute disseminated encephalomyelitis (ADEM)-like pathology. *Acta Neuropathol* **140**, 1–6 (2020).
24. Koralnik, I.J. & Tyler, K.L. COVID-19: A Global Threat to the Nervous System. *Ann Neurol* **88**, 1–11 (2020).
25. Shin, D., *et al.* Papain-like protease regulates SARS-CoV-2 viral spread and innate immunity. *Nature* (2020).
26. Bojkova, D., *et al.* Proteomics of SARS-CoV-2-infected host cells reveals therapy targets. *Nature* **583**, 469–472 (2020).
27. Zhang, L., *et al.* Crystal structure of SARS-CoV-2 main protease provides a basis for design of improved alpha-ketoamide inhibitors. *Science* **368**, 409–412 (2020).
28. Wu, J. & Chen, Z.J. Innate immune sensing and signaling of cytosolic nucleic acids. *Annu Rev Immunol* **32**, 461–488 (2014).
29. Kondylis, V., Kumari, S., Vlantis, K. & Pasparakis, M. The interplay of IKK, NF-kappaB and RIPK1 signaling in the regulation of cell death, tissue homeostasis and inflammation. *Immunol Rev* **277**, 113–127 (2017).
30. Hamming, I., *et al.* Tissue distribution of ACE2 protein, the functional receptor for SARS coronavirus. A first step in understanding SARS pathogenesis. *J Pathol* **203**, 631–637 (2004).
31. Hoffmann, M., *et al.* SARS-CoV-2 Cell Entry Depends on ACE2 and TMPRSS2 and Is Blocked by a Clinically Proven Protease Inhibitor. *Cell* **181**, 271–280 e278 (2020).

32. Zhou, P., *et al.* A pneumonia outbreak associated with a new coronavirus of probable bat origin. *Nature* **579**, 270–273 (2020).
33. Jiang, H.W., *et al.* SARS-CoV-2 proteome microarray for global profiling of COVID-19 specific IgG and IgM responses. *Nat Commun* **11**, 3581 (2020).
34. Audry, M., *et al.* NEMO is a key component of NF-kappaB- and IRF-3-dependent TLR3-mediated immunity to herpes simplex virus. *The Journal of allergy and clinical immunology* **128**, 610–617 e611-614 (2011).
35. Krichel, B., Falke, S., Hilgenfeld, R., Redecke, L. & Uetrecht, C. Processing of the SARS-CoV pp1a/ab nsp7-10 region. *Biochem J* **477**, 1009–1019 (2020).
36. Buszko, M., *et al.* The dynamic changes in cytokine responses in COVID-19: a snapshot of the current state of knowledge. *Nat Immunol* **21**, 1146–1151 (2020).
37. Körbelin, J., *et al.* A brain microvasculature endothelial cell-specific viral vector with the potential to treat neurovascular and neurological diseases. *EMBO Molecular Medicine* **8**, 609–625 (2016).
38. Brown, W.R. A review of string vessels or collapsed, empty basement membrane tubes. *J Alzheimers Dis* **21**, 725–739 (2010).
39. Ridder, D.A., *et al.* Brain endothelial TAK1 and NEMO safeguard the neurovascular unit. *J Exp Med* **212**, 1529–1549 (2015).
40. Rothhammer, V., *et al.* Microglial control of astrocytes in response to microbial metabolites. *Nature* **557**, 724–728 (2018).
41. Villasenor, R., *et al.* Trafficking of Endogenous Immunoglobulins by Endothelial Cells at the Blood-Brain Barrier. *Scientific reports* **6**, 25658 (2016).
42. Villasenor, R., *et al.* Region-specific permeability of the blood-brain barrier upon pericyte loss. *J Cereb Blood Flow Metab* **37**, 3683–3694 (2017).
43. Troyer, E.A., Kohn, J.N. & Hong, S. Are we facing a crashing wave of neuropsychiatric sequelae of COVID-19? Neuropsychiatric symptoms and potential immunologic mechanisms. *Brain Behav Immun* **87**, 34–39 (2020).
44. Zhang, J., *et al.* A systemic and molecular study of subcellular localization of SARS-CoV-2 proteins. *bioRxiv*, 2020.2008.2002.233023 (2020).
45. Miyamoto, S. Nuclear initiated NF-kappaB signaling: NEMO and ATM take center stage. *Cell Res* **21**, 116–130 (2011).
46. Arunachalam, P.S., *et al.* Systems biological assessment of immunity to mild versus severe COVID-19 infection in humans. *Science* **369**, 1210–1220 (2020).
47. Hadjadj, J., *et al.* Impaired type I interferon activity and inflammatory responses in severe COVID-19 patients. *Science* **369**, 718–724 (2020).
48. Wang, D., *et al.* Porcine Epidemic Diarrhea Virus 3C-Like Protease Regulates Its Interferon Antagonism by Cleaving NEMO. *J Virol* **90**, 2090–2101 (2016).

49. Zhu, X., *et al.* Porcine deltacoronavirus nsp5 inhibits interferon-beta production through the cleavage of NEMO. *Virology* **502**, 33–38 (2017).
50. Chen, S., *et al.* Feline Infectious Peritonitis Virus Nsp5 Inhibits Type I Interferon Production by Cleaving NEMO at Multiple Sites. *Viruses* **12**(2019).
51. Colmenero, I., *et al.* SARS-CoV-2 endothelial infection causes COVID-19 chilblains: histopathological, immunohistochemical and ultrastructural study of seven paediatric cases. *The British journal of dermatology* (2020).
52. Gareus, R., *et al.* Endothelial cell-specific NF-kappaB inhibition protects mice from atherosclerosis. *Cell Metab* **8**, 372–383 (2008).
53. van Loo, G., *et al.* Inhibition of transcription factor NF-kB in the central nervous system ameliorates autoimmune encephalomyelitis in mice. *Nat. Immunol.* **7**, 954–961 (2006).
54. Minic, S., Trpinac, D. & Obradovic, M. Systematic review of central nervous system anomalies in incontinentia pigmenti. *Orphanet journal of rare diseases* **8**, 25 (2013).
55. Meuwissen, M.E. & Mancini, G.M. Neurological findings in incontinentia pigmenti; a review. *Eur J Med Genet* **55**, 323–331 (2012).
56. Kanberg, N., *et al.* Neurochemical evidence of astrocytic and neuronal injury commonly found in COVID-19. *Neurology* **95**, e1754-e1759 (2020).
57. Senatorov, V.V., Jr., *et al.* Blood-brain barrier dysfunction in aging induces hyperactivation of TGFbeta signaling and chronic yet reversible neural dysfunction. *Sci Transl Med* **11**, eaaw8283 (2019).
58. Martens, S., Hofmans, S., Declercq, W., Augustyns, K. & Vandenabeele, P. Inhibitors Targeting RIPK1/RIPK3: Old and New Drugs. *Trends Pharmacol Sci* **41**, 209–224 (2020).
59. Mifflin, L., Ofengeim, D. & Yuan, J. Receptor-interacting protein kinase 1 (RIPK1) as a therapeutic target. *Nat Rev Drug Discov* **19**, 553–571 (2020).
60. Grievink, H.W., *et al.* DNL104, a Centrally Penetrant RIPK1 Inhibitor, Inhibits RIP1 Kinase Phosphorylation in a Randomized Phase I Ascending Dose Study in Healthy Volunteers. *Clin Pharmacol Ther* **107**, 406–414 (2020).
61. Nampoothiri, S., *et al.* The hypothalamus as a hub for SARS-CoV-2 brain infection and pathogenesis. *bioRxiv*, 2020.2006.2008.139329 (2020).

Figures

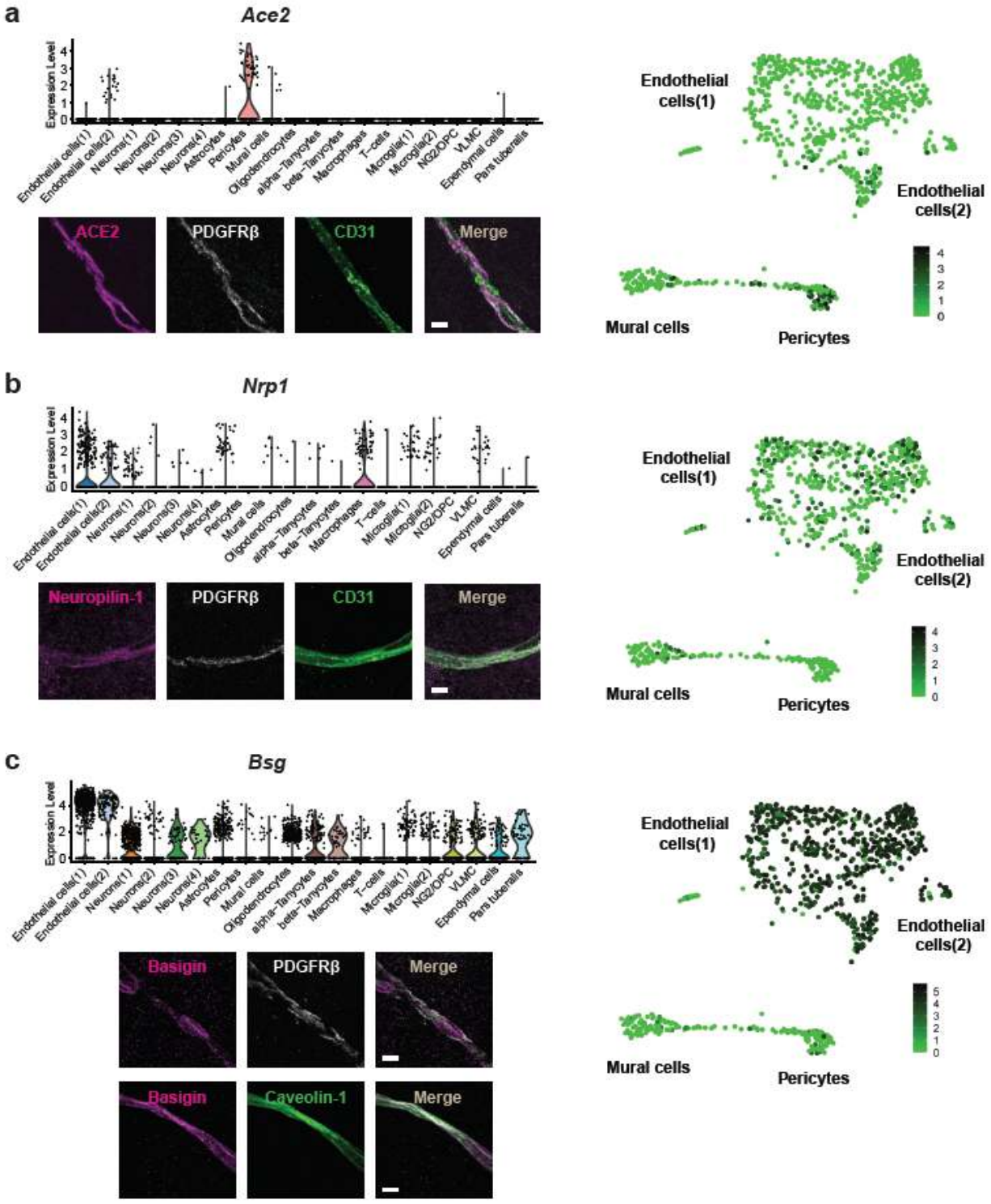

Figure 1

Brain endothelial cells express SARS-CoV-2 receptors. a, RNA sequencing in single mouse brain cells demonstrated that Ace2 mRNA was mainly expressed in pericytes and endothelial cell cluster 2. Gene expression is shown as violin plots for all 20 clusters and as part of the UMAP plot containing endothelial, pericytic, and mural clusters (boxed area in the complete UMAP plot shown in Extended data Fig. 1a). Gene expression levels are color-coded. Co-staining of ACE2 with the endothelial marker CD31

and the pericyte marker PDGFRβ confirmed the cell type-specific localization of the receptors in the vascular unit. Representative images of the mouse brain are shown. Note that in the single-cell RNA-seq analysis, the number of Ace2 mRNA-positive cells was low and did not fully reflect the number of ACE2 protein-positive cells identified by immunostainings. In immunostainings, almost all pericytes (identified by co-localization with PDGFRβ) and tanycytes61 were positive for ACE2, in contrast to the single-cell RNA sequence data. b, Nrp1 mRNA was expressed mainly in endothelial cells, some neurons, astrocytes, and macrophages. Neuropilin-1 was co-localized with the endothelial marker CD31 but not with the pericyte marker PDGFRβ. Representative images of the mouse brain are shown. c, Bsg was highly expressed in endothelial cells, neurons, and astrocytes, whereas only few pericytes and mural cells expressed Bsg. BSG was co-localized with the endothelial protein caveolin-1 but not with PDGFRβ. Representative images of the mouse brain are shown. Scale bars, 5 μm. VLMC, vascular and leptomeningeal cells; OPC, oligodendrocyte progenitor cells.

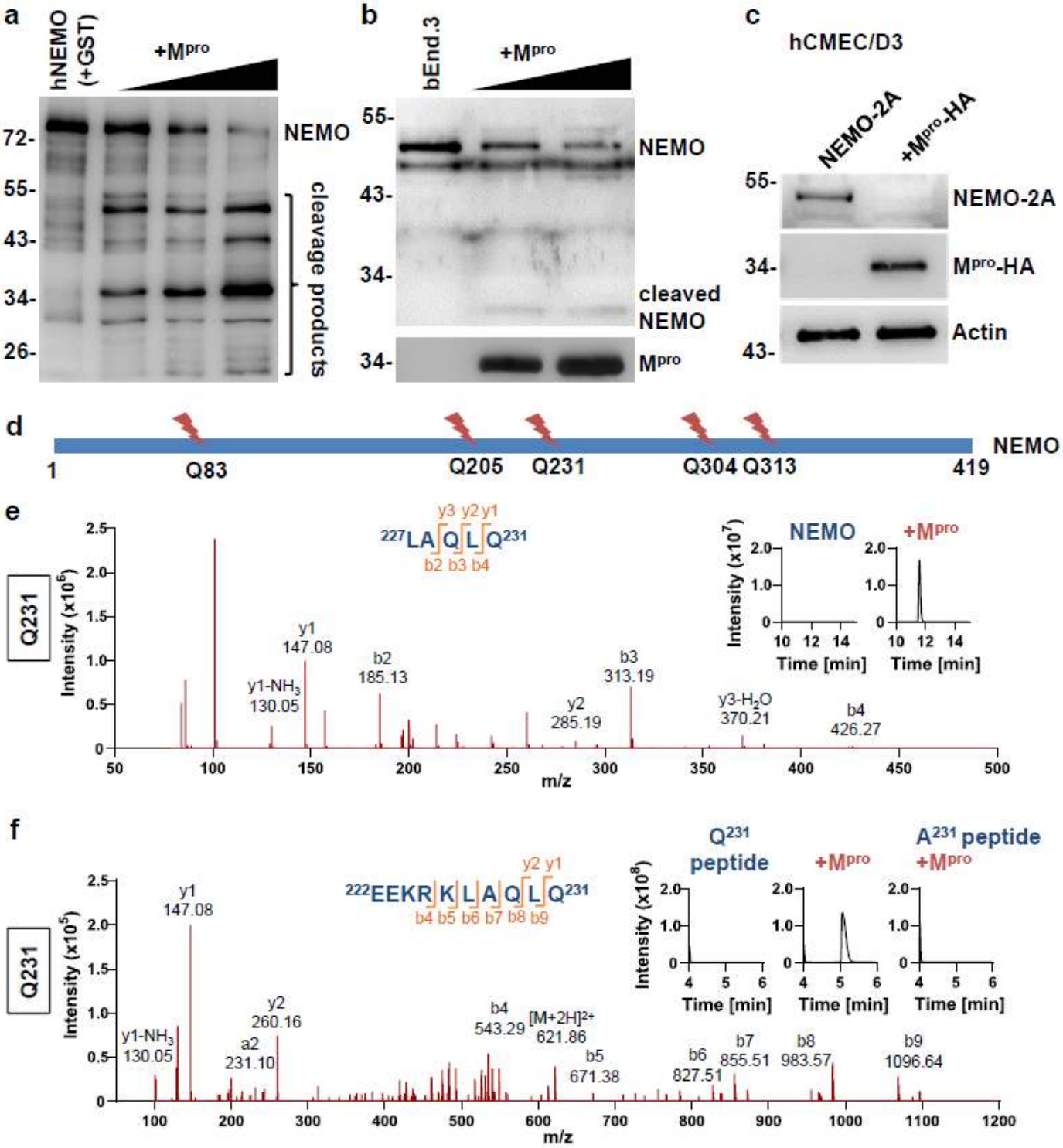

Figure 2

Mpro cleaves NEMO. a, Increasing concentrations of SARS-CoV-2 Mpro (0, 5, 10, 25 μM; 120 min) degraded full-length human NEMO (fused to GST) while several cleavage products emerged. Full blots are shown in Extended data Fig. 2. b, Mouse NEMO in bEnd.3 cell extracts was cleaved to a short fragment after incubation with increasing concentrations of Mpro (0, 5, 10 μM) for 120 min. c, In human brain endothelial hCMEC/D3 cells, Mpro-HA degraded NEMO-2A. After transfecting the cells with pCAG-

NEMO-2A-GFP ± pCAG-Mpro-HA, immunoblots of cell lysates were performed. Mpro-HA expression did not affect GFP expression (Extended data Fig. 3c). d, Tryptic digestion and MS/MS analysis identified five Mpro cleavage sites in human NEMO that are illustrated in a scheme. For the protein sequence, see Extended data Fig. 4k. e, Mpro cleaved human NEMO at Q231. An extracted ion chromatogram (EIC) of the tryptic peptide 227LAQLQ231 (m/z, 572.34142+; retention time [RT], 11.6 min) derived from NEMO after incubation with Mpro (5 µM, inset) and the MS/MS spectrum that was used for peptide identification are shown. f, A synthetic peptide corresponding to the human NEMO sequence confirmed that Q231 is an Mpro cleavage site. Total ion chromatograms after incubation of the synthetic peptide h-NEMO_222-241 (EEKRKLAQLQVAYHQLFQEY) in the presence or absence of Mpro (2.5 µM, inset) are shown. In the presence of Mpro, the proteolysis product 222EEKRKLAQLQ231 (m/z, 414.91093+; RT, 5.1 min) was detected. The mutant peptide h-NEMO-Q231A_222-241 (EEKRKLAQLAVAYHQLFQEY) was not cleaved by Mpro (inset). The MS/MS spectrum of the peptide 222EEKRKLAQLQ231 is shown.

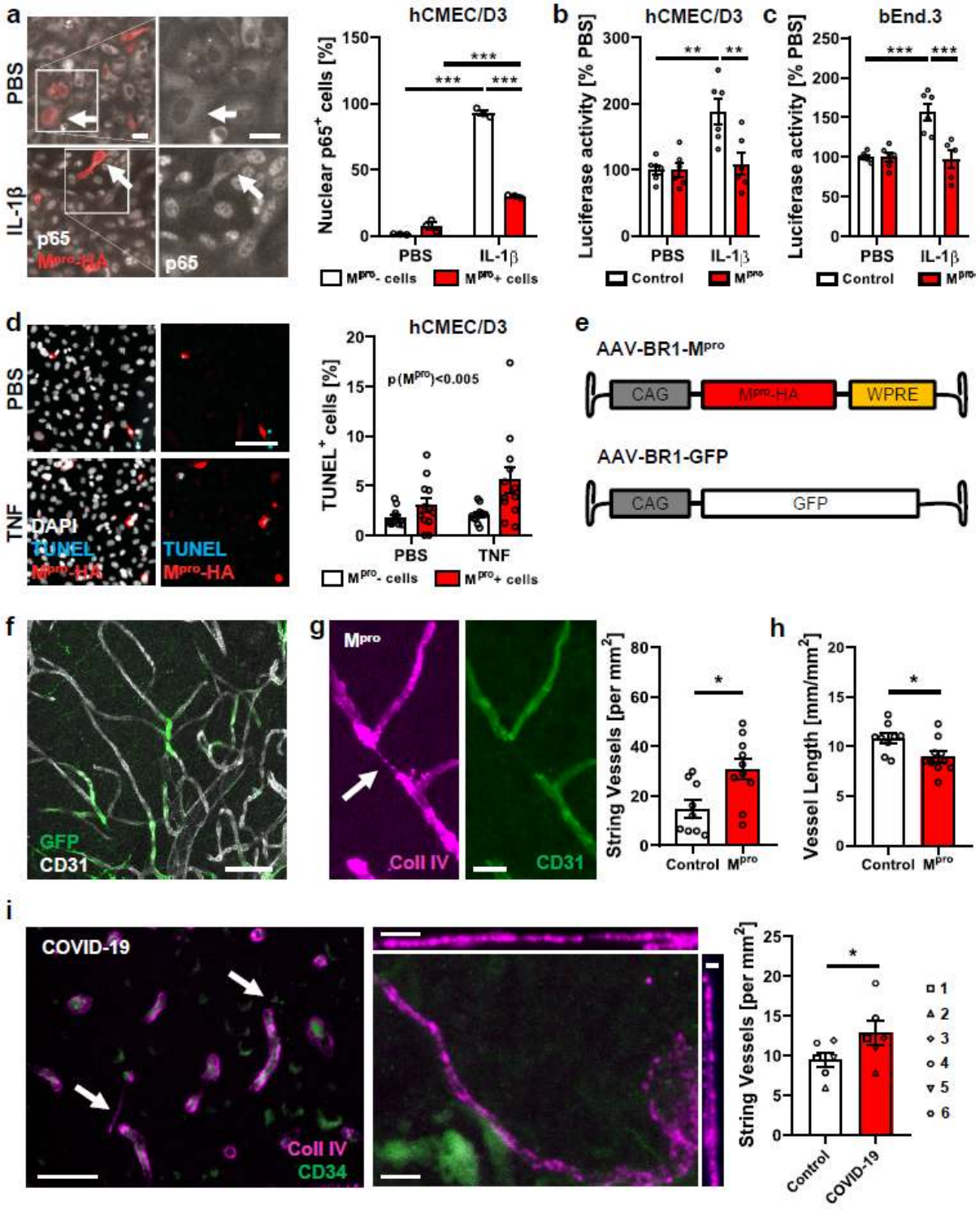

Figure 3

Mpro inactivates NEMO and induces brain endothelial cell loss mimicking COVID-19-associated brain pathology. a, Mpro-HA inhibited the nuclear translocation of the NF-κB subunit p65 reflecting NF-κB activation when hCMEC/D3 cells were stimulated with IL-1β (0.25 µg/ml) for 30 min. Cells were transfected with pCAG-Mpro-HA. Two-way ANOVA followed by Tukey's post-hoc test (Mpro: $F(1,8) = 467.3$, $p < 0.0001$; treatment: $F(1,8) = 1801.0$, $p < 0.0001$; interaction: $F(1,8) = 671.9$, $p < 0.0001$; N = 3

wells/group; representative for 3 independent experiments). Scale bar, 25 μm. b, c, Mpro-HA blocked the activation of NF-κB by IL-1β (0.25 μg/ml) in human (b) and mouse (c) brain endothelial cells. Cells were transfected with pNFkB-Luc ± pCAG-Mpro-HA and luciferase activity was determined as a measure of NF-κB activity. Two-way ANOVA followed by Tukey's post-hoc test (hCMEC/D3: Mpro: $F(1,20) = 7.8$, $p = 0.011$; treatment: $F(1,20) = 11.5$, $p = 0.003$; interaction: $F(1,20) = 7.8$, $p = 0.011$; N = 6 wells/group; bEND.3: Mpro: $F(1,19) = 13.8$, $p = 0.002$; treatment: $F(1,19) = 10.9$, $p = 0.004$; interaction: $F(1,19) = 13.8$, $p = 0.002$; N = 5-6 wells/group). d, Mpro-HA induced death of hCMEC/D3 cells, especially after exposure to TNF (100 ng/ml, 4.5 hours). Scheirer-Ray-Hare test (Mpro: $\chi2(1) = 8.2$, $p < 0.005$; treatment: $\chi2(1) = 2.9$, $p > 0.05$; interaction: $\chi2(1) = 0.3$, $p > 0.05$; N = 12 wells/group). Scale bar, 100 μm. e, Scheme of AAV-BR1 vectors used to transduce brain endothelial cells in vivo. WPRE, woodchuck hepatitis post-transcriptional regulatory element. f, After injecting the control vector AAV-BR1-GFP into mice, brain endothelial cells expressed GFP. Scale bar, 50 μm. g, AAV-BR1-Mpro led to the formation of empty basement membrane tubes, also known as string vessels, in the brain of mice. String vessels were identified as thin collagen IV (Coll IV)+ vessels that were negative for the endothelial marker CD31. Representative images taken in the cortex and the quantification of string vessel length in percent of total vessel length are shown. Two-tailed unpaired t test, $T(17) = 2.9$, $p = 0.010$, N = 9-10 animals/group. Scale bar, 25 μm. h, Total vessel length was reduced after mice received AAV-BR1-Mpro. Two-tailed unpaired t test, $T(17) = 2.6$, $p = 0.021$, N = 9-10 animals/group. i, In brains of SARS-CoV-2-infected patients, string vessels were increased in the frontal cortex. Sections were stained for the basement membrane marker Coll IV and the endothelial marker CD34. The patient IDs of SARS-CoV-2 and sex- and age-matched control patients refer to Extended data Table 1. Two-tailed Wilcoxon signed rank test, $p = 0.031$. Scale bars, 50 μm (left panel), 3 μm (right panel). * $p < 0.05$; ** $p < 0.01$; ***$p < 0.001$. All data are shown as means ± SEM.

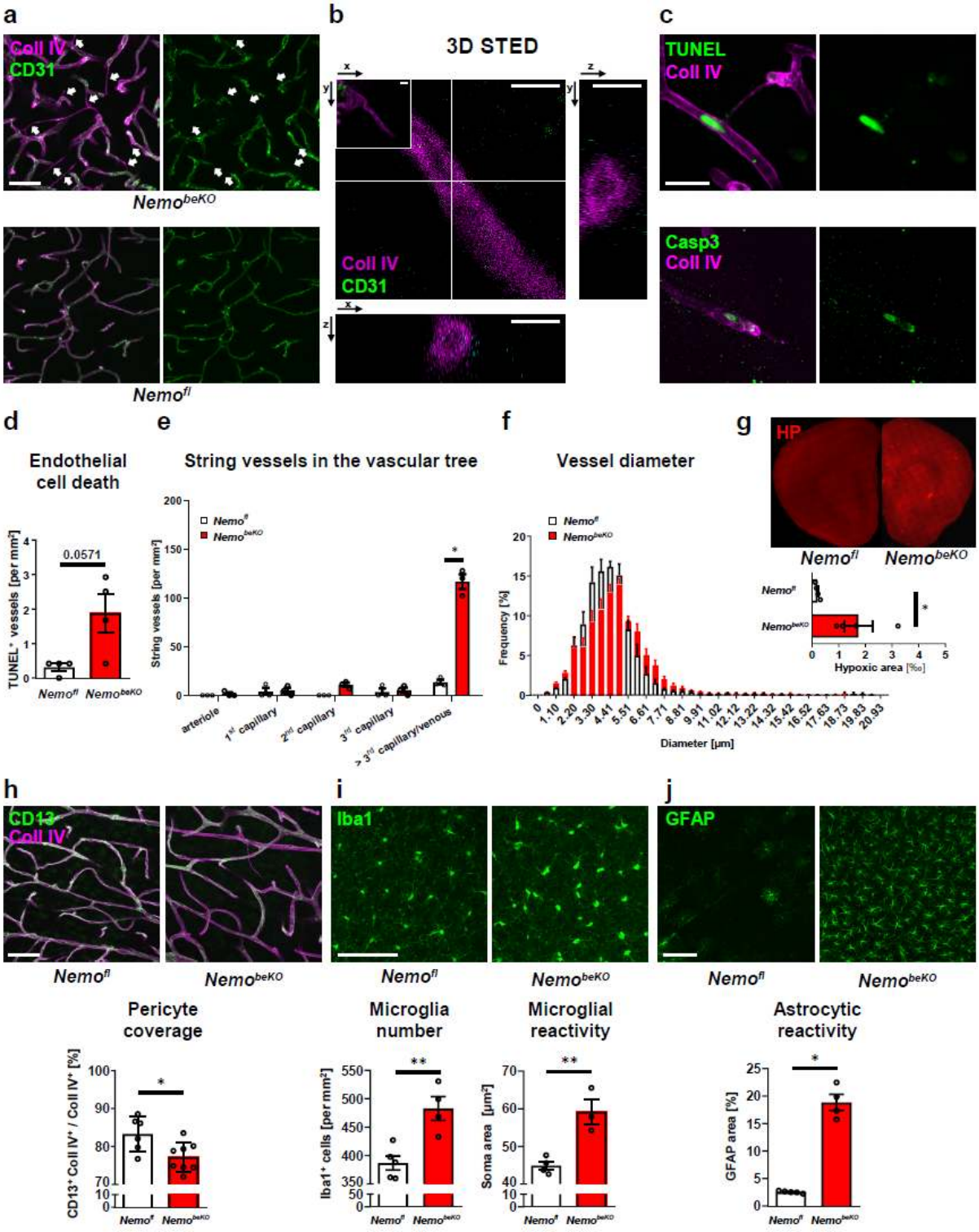

Figure 4

Brain endothelial loss of NEMO induces string vessel formation and influences the neurovascular unit. a, Cerebral vasculature of NemobeKO mice compared to Nemofl controls. NemobeKO animals are deficient of NEMO in brain endothelial cells. String vessels were identified as thin collagen IV (Coll IV)+ vessels that were negative for the endothelial marker CD31. White arrows indicate the massive occurrence of string vessels in NemobeKO mice. Scale bar, 50 µm. b, STED microscopy showed that string vessels are thin

tubes with a typical diameter of 0.5 – 1 µm. Scale bars, 1 µm. c, String vessels were often adjacent to dying, TUNEL+ or active caspase-3+ endothelial cells in NemobeKO mice. Scale bar, 20 µm. d, Counting of TUNEL+ vessels revealed a tendency towards increased endothelial cell death in NemobeKO mice. One-tailed Mann-Whitney U test, $p = 0.057$, N = 4 animals/group. e, More string vessels were present in higher branched orders of the vascular tree in NemobeKO mice. String vessels positive for α-SMA are defined as arterial string vessels, adjacent string vessels as 1st order capillary string vessels, etc. (see also Extended data Fig. 7b). Repeated measures ANOVA followed by Sidak's post-hoc test (genotype: $F(1,4) = 163.3$, $p < 0.001$; branch order: $F(4,16) = 123.5$, $p < 0.001$; interaction: $F(4,16) = 81.2$, $p < 0.001$; N = 3 animals/group). f, NemobeKO mice preferentially lost vessels with small diameters. The diameters of Collagen (Coll) IV+ vessels are shown as a histogram (N = 3 animals). g, NemobeKO mice demonstrated patchy cerebral hypoxia that was quantified by measuring the hypoxic area, as stained by the hypoxia probe (HP). Two-tailed Mann-Whitney U test, $p = 0.029$, N = 4 animals/group (mean of 4 images/animal). h, Pericyte coverage of vessels (CD13+ area in Coll IV+ vessels as percentage of the total area of the vessels) was reduced in NemobeKO mice. Scale bar, 100 µm. Two-tailed unpaired t test, $T(12) = 2.7$, $p = 0.019$, N = 6-8 animals/group. i, NemobeKO mice showed an increase in the number of microglia cells that were activated as shown by significantly increased Iba1+ soma area. Scale bar, 100 µm. Two-tailed unpaired t test, $T(7) = 4.1$, $p = 0.004$, and $T(2.4) = 4.1$ (Welch corrected), $p = 0.039$, N = 3-5 animals/group. j, NemobeKO mice demonstrated astrogliosis as shown by a significantly increased GFAP+ area in the cortex. Scale bar, 100 µm. Two-tailed unpaired t test, Welch corrected, $T(3.0) = 11.1$, $p = 0.002$, N = 4-5 animals/group. * $p < 0.05$; ** $p < 0.01$. All data are shown as means ± SEM.

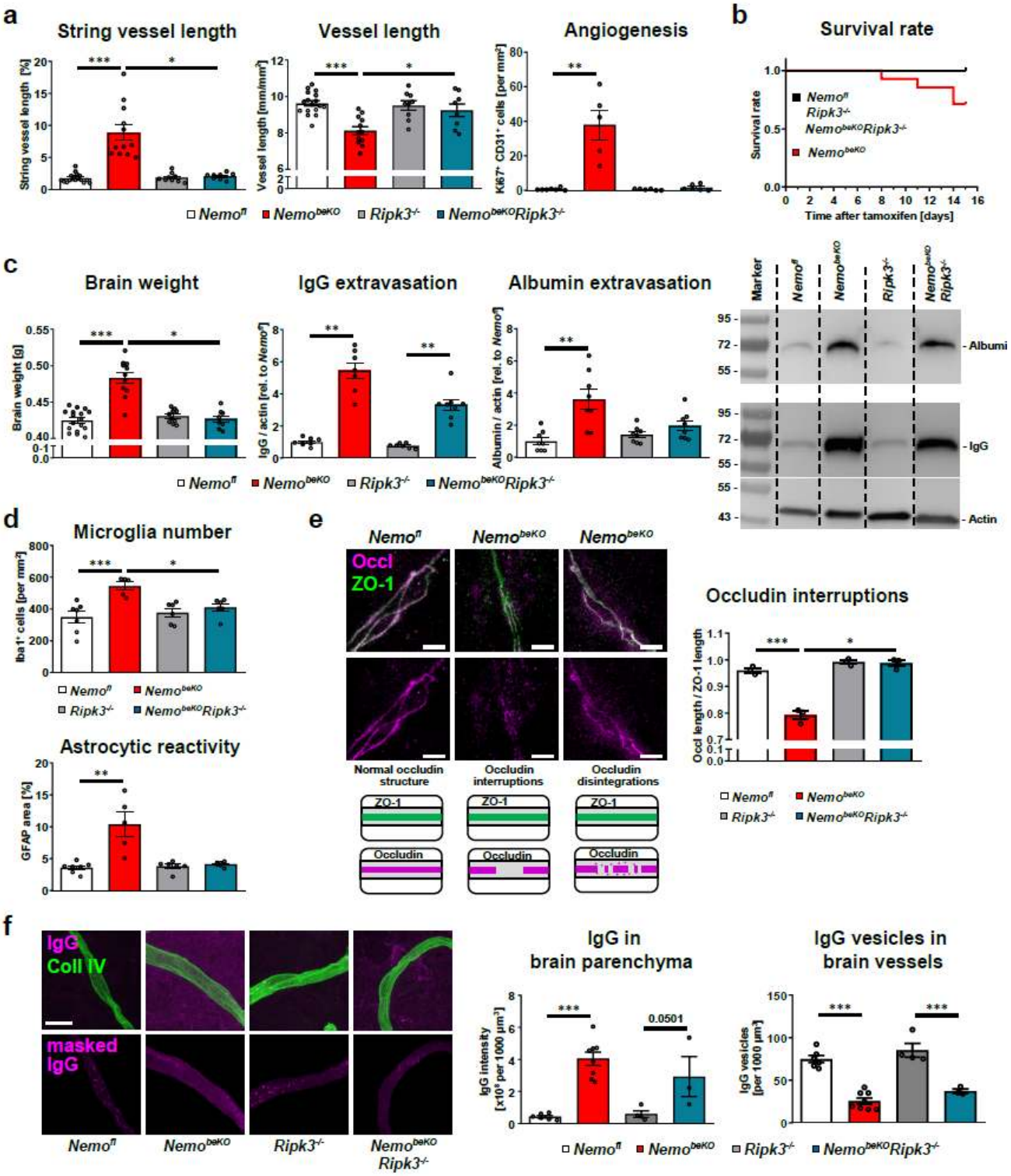

Figure 5

Brain endothelial loss of NEMO induces string vessel formation and influences the neurovascular unit. a, Cerebral vasculature of NemobeKO mice compared to Nemofl controls. NemobeKO animals are deficient of NEMO in brain endothelial cells. String vessels were identified as thin collagen IV (Coll IV)+ vessels that were negative for the endothelial marker CD31. White arrows indicate the massive occurrence of string vessels in NemobeKO mice. Scale bar, 50 µm. b, STED microscopy showed that string vessels are thin

tubes with a typical diameter of 0.5 – 1 µm. Scale bars, 1 µm. c, String vessels were often adjacent to dying, TUNEL+ or active caspase-3+ endothelial cells in NemobeKO mice. Scale bar, 20 µm. d, Counting of TUNEL+ vessels revealed a tendency towards increased endothelial cell death in NemobeKO mice. One-tailed Mann-Whitney U test, $p = 0.057$, N = 4 animals/group. e, More string vessels were present in higher branched orders of the vascular tree in NemobeKO mice. String vessels positive for α-SMA are defined as arterial string vessels, adjacent string vessels as 1st order capillary string vessels, etc. (see also Extended data Fig. 7b). Repeated measures ANOVA followed by Sidak's post-hoc test (genotype: $F(1,4) = 163.3$, $p < 0.001$; branch order: $F(4,16) = 123.5$, $p < 0.001$; interaction: $F(4,16) = 81.2$, $p < 0.001$; N = 3 animals/group). f, NemobeKO mice preferentially lost vessels with small diameters. The diameters of Collagen (Coll) IV+ vessels are shown as a histogram (N = 3 animals). g, NemobeKO mice demonstrated patchy cerebral hypoxia that was quantified by measuring the hypoxic area, as stained by the hypoxia probe (HP). Two-tailed Mann-Whitney U test, $p = 0.029$, N = 4 animals/group (mean of 4 images/animal). h, Pericyte coverage of vessels (CD13+ area in Coll IV+ vessels as percentage of the total area of the vessels) was reduced in NemobeKO mice. Scale bar, 100 µm. Two-tailed unpaired t test, $T(12) = 2.7$, $p = 0.019$, N = 6-8 animals/group. i, NemobeKO mice showed an increase in the number of microglia cells that were activated as shown by significantly increased Iba1+ soma area. Scale bar, 100 µm. Two-tailed unpaired t test, $T(7) = 4.1$, $p = 0.004$, and $T(2.4) = 4.1$ (Welch corrected), $p = 0.039$, N = 3-5 animals/group. j, NemobeKO mice demonstrated astrogliosis as shown by a significantly increased GFAP+ area in the cortex. Scale bar, 100 µm. Two-tailed unpaired t test, Welch corrected, $T(3.0) = 11.1$, $p = 0.002$, N = 4-5 animals/group. * $p < 0.05$; ** $p < 0.01$. All data are shown as means ± SEM.

Supplementary Files

This is a list of supplementary files associated with this preprint. Click to download.

- 20201002NSP5Extendeddatasubmitted.docx
- ExtendeddataFigure19.pdf